Diagnostic Comparison of Meteorological Analyses during the 2002 Antarctic Winter

GLORIA L. MANNEY,[a,*] DOUGLAS R. ALLEN,[b] KRISTIN KRÜGER,[c,+] BARBARA NAUJOKAT,[c]
MICHELLE L. SANTEE,[a] JOSEPH L. SABUTIS,[d] STEVEN PAWSON,[e,f] RICHARD SWINBANK,[g]
CORA E. RANDALL,[h] ADRIAN J. SIMMONS,[i] AND CRAIG LONG[j]

[a]*Jet Propulsion Laboratory, California Institute of Technology, Pasadena, California*
[b]*Remote Sensing Division, Naval Research Laboratory, Washington, D.C.*
[c]*Institut für Meteorologie, Freie Universität Berlin, Berlin, Germany*
[d]*School of Education and Department of Mathematical Sciences, New Mexico Highlands University, Las Vegas, New Mexico*
[e]*NASA Goddard Space Flight Center, Greenbelt, Maryland*
[f]*Goddard Earth Science and Technology Center, University of Maryland, Baltimore County, Baltimore, Maryland*
[g]*Met Office, Exeter, Devon, United Kingdom*
[h]*Laboratory for Atmospheric and Space Physics, University of Colorado, Boulder, Colorado*
[i]*European Centre for Medium-Range Weather Forecasts, Reading, United Kingdom*
[j]*NOAA/Climate Prediction Center, Camp Springs, Maryland*

(Manuscript received 27 July 2004, in final form 4 November 2004)

ABSTRACT

Several meteorological datasets, including U.K. Met Office (MetO), European Centre for Medium-Range Weather Forecasts (ECMWF), National Centers for Environmental Prediction (NCEP), and NASA's Goddard Earth Observation System (GEOS-4) analyses, are being used in studies of the 2002 Southern Hemisphere (SH) stratospheric winter and Antarctic major warming. Diagnostics are compared to assess how these studies may be affected by the meteorological data used. While the overall structure and evolution of temperatures, winds, and wave diagnostics in the different analyses provide a consistent picture of the large-scale dynamics of the SH 2002 winter, several significant differences may affect detailed studies. The NCEP–NCAR reanalysis (REAN) and NCEP–Department of Energy (DOE) reanalysis-2 (REAN-2) datasets are not recommended for detailed studies, especially those related to polar processing, because of lower-stratospheric temperature biases that result in underestimates of polar processing potential, and because their winds and wave diagnostics show increasing differences from other analyses between ~30 and 10 hPa (their top level). Southern Hemisphere polar stratospheric temperatures in the ECMWF 40-Yr Re-analysis (ERA-40) show unrealistic vertical structure, so this long-term reanalysis is also unsuited for quantitative studies. The NCEP/Climate Prediction Center (CPC) objective analyses give an inferior representation of the upper-stratospheric vortex. Polar vortex transport barriers are similar in all analyses, but there is large variation in the amount, patterns, and timing of mixing, even among the operational assimilated datasets (ECMWF, MetO, and GEOS-4). The higher-resolution GEOS-4 and ECMWF assimilations provide significantly better representation of filamentation and small-scale structure than the other analyses, even when fields gridded at reduced resolution are studied. The choice of which analysis to use is most critical for detailed transport studies (including polar process modeling) and studies involving synoptic evolution in the upper stratosphere. The operational assimilated datasets are better suited for most applications than the NCEP/CPC objective analyses and the reanalysis datasets (REAN/REAN-2 and ERA-40).

1. Introduction

The first major stratospheric sudden warming observed in the Southern Hemisphere (SH) occurred in late September 2002 (e.g., Allen et al. 2003; see special issue of *Journal of the Atmospheric Sciences,* vol. 62, no. 3, hereinafter *JAS*). The stratospheric circulation throughout that winter was much more dynamically disturbed than in any other SH winter since the establishment of comprehensive upper-air observations in 1979 (e.g., Allen et al. 2003; Roscoe et al. 2005). Because of its uniqueness, the 2002 winter has been and continues to be the subject of intensive study, including examination of transport, ozone chemistry, the dynamics of and mechanisms leading to the major warming, and the unusual dynamical situation throughout the winter.

Nearly all of these studies rely on meteorological analyses (temperatures, geopotential height, and wind data) from one or more operational or reanalysis as-

* Additional affiliation: Department of Natural Sciences, New Mexico Highlands University, Las Vegas, New Mexico.
+ Current affiliation: Alfred Wegener Institute for Polar and Marine Research, Potsdam, Germany.

Corresponding author address: Gloria Manney, Department of Natural Sciences, New Mexico Highlands University, Las Vegas, NM 87701.
E-mail: manney@mls.jpl.nasa.gov

TABLE 1. Characteristics of meteorological analyses used in the intercomparisons, from ECMWF operational forecasts, ERA-40, special ECMWF runs (ECMWF-R), NASA GMAO's GEOS Version 4.03 (GEOS-4), GEOS-4 Version 4.02 (GEOS-4P), GEOS-4 Version 4.02 reduced resolution (GEOS-4L), the NCEP/CPC, MetO, REAN, and REAN-2. T(number) refers to the triangular wavenumber truncation of a spectral model. Grids are given as latitude × longitude. PSAS is Physical Space Statistical Analysis Scheme. Levels are given as number, top pressure level. The primary product used from each center is given in italics.

Product	Analysis method	Analysis grid	Output grid	Model levels	Output levels	Output times (UTC)	Reference(s)
ECMWF	4DVAR	T511 (~40 km)	2.5° × 2.5°	60, 0.1 hPa	20, 1 hPa	0000, 0600, 1200, 1800	Simmons et al. (2005)
ERA-40	3DVAR	T159m (~125 km)	2.5° × 2.5°	60, 0.1 hPa	23, 1 hPa	0000, 0600, 1200, 1800	Simmons et al. (2005)
ECMWF-R	4DVAR	T511 (~40 km)	1.25° × 1.25°	60, 0.1 hPa	23, 1 hPa	0000, 0600, 1200, 1800	Simmons et al. (2005)
GEOS-4	PSAS	1.0° × 1.25°	1.0° × 1.25°	55, 0.01 hPa	55, 0.01 hPa	0000, 0600, 1200, 1800 (6-h avg)	Lin (2004); LBPL
GEOS-4P	PSAS	1.0° × 1.25°	1.0° × 1.25°	55, 0.01 hPa	36, 0.2 hPa	0000, 0600, 1200, 1800	
GEOS-4L	PSAS	1.0° × 1.25°	2.0° × 2.5°	55, 0.01 hPa	36, 0.2 hPa	1200	
MetO	3DVAR	2.5° × 3.75°	2.5° × 3.75°	40, 0.1 hPa	22, 0.32 hPa	1200	Swinbank et al. (2002)
NCEP/CPC	3DVAR	T254 (~80 km)	2.5° × 5.0°	64, 0.2 hPa	14, 10 hPa	1200	
	Objective analysis	65 × 65PS		5–0.4 hPa	4, 0.4 hPa		Finger et al. (1993); Gelman et al. (1994)
REAN	3DVAR	T62 (~300 km)	2.5° × 2.5°	28, 3 hPa	17, 10 hPa	1200 (24-h avg)	Kalnay et al. (1996); Kistler et al. (2001)
REAN-2	3DVAR	T62 (~300 km)	2.5° × 2.5°	28, 3 hPa	17, 10 hPa	1200 (24-h avg)	Kanamitsu et al. (2002)

similation systems. Manney et al. (2003) showed for the Northern Hemisphere (NH) winter lower stratosphere that significant differences in the results of polar processing studies were expected depending on the dataset used, and that the differences between datasets depended on the particular meteorological conditions. While several studies have examined differences between meteorological datasets in the Arctic (see references in Manney et al. 2003), few comparisons have focused on the SH winter. Interhemispheric differences in agreement among the analyses might be expected: While the satellite data inputs to the analyses are global, the ground-based data available are much sparser in the SH; thus the analyses are not as well constrained by data. On the other hand, the typically cold, quiescent conditions of the SH winter are inherently more predictable than those in the NH winter, and thus require fewer observations to adequately constrain the analysis systems. The unusual and pronounced dynamical activity in the 2002 winter might thus result in more significant differences between meteorological analyses than are typical in the SH.

We compare here the most commonly used meteorological datasets during the 2002 SH winter, focusing on diagnostics that are representative of calculations done in several types of scientific studies, including those of large-scale dynamics and wave propagation, synoptic evolution, transport barriers, mixing and filamentation, and polar processing. By choosing diagnostics related to those used in scientific studies, we hope to elucidate some areas of uncertainty resulting from differences in the analyses and provide some guidance as to the appropriateness of various datasets for particular types of studies.

2. Data and analysis

The meteorological datasets we have examined are summarized in Table 1. Several of these datasets are described by Manney et al. (2003) and Randel et al. (2004), but there have been some changes since then: The National Centers for Environmental Prediction/Climate Prediction Center (NCEP/CPC) analyses now use data from the Global Data Assimilation System (GDAS; NCEP's operational assimilation system) interpolated to the 65 × 65 polar stereographic grid used for the upper-stratospheric objective analyses at all levels up to 10 hPa; however, only geopotential heights and temperatures are provided, so the winds at all levels are still calculated using a "balance wind" formulation (Randel 1987; Newman et al. 1989; Manney et al. 1996). The 2002 U.K. Met Office (MetO) analyses are from a three-dimensional variational data assimilation (3DVAR) system that assimilates satellite radiances (e.g., Lorenc et al. 2000; Swinbank et al. 2002). European Centre for Medium-Range Weather Forecasts (ECMWF), Global Modeling and Assimilation Office (GMAO), and GDAS systems also assimilate satellite radiances rather than retrieved temperatures. The resolution of the operational ECMWF analyses for the 2002 SH winter is T511, in contrast to T319 for earlier studies. The ECMWF-R reruns listed in Table 1 are from a version that became operational in January 2003; results from these closely resemble those from ECMWF for all of the diagnostics shown here. The National Aeronautics and Space Administration's (NASA) GMAO system, the Goddard Earth Observation System (GEOS-4.0.2), became operational in October 2002, and the 2002 winter was reprocessed with that

system, then again with the final version, GEOS-4.0.3 (referred to hereinafter as GEOS-4). The diagnostics discussed here were initially done using GEOS-4.0.2 (GEOS-4P) and were compared with GEOS-4.0.2 on a coarser grid (GEOS-4L) to examine resolution effects.

The NCEP–National Center for Atmospheric Research (NCAR) reanalysis-2 (REAN-2) uses the same underlying assimilation model as the first reanalysis (REAN), but with several corrections, as described by Kanamitsu et al. (2002). It still has many of the same limitations, including low-resolution, older forecast model, assimilation of retrieved temperatures rather than radiances, 3DVAR rather than four-dimensional variational data assimilation (4DVAR), poor vertical resolution in the stratosphere, and a top analysis level at 10 hPa. Results for REAN and REAN-2 data are much more similar to each other than either one is to the other analyses. ECMWF 40-Yr Re-analysis (ERA-40) data were produced through August 2002; they have been used for a number of analyses in the SH stratosphere, including assessing whether events comparable to the 2002 major warming may have occurred previously in the SH (e.g., Simmons et al. 2005). In August 2002, but not in the previous months of that winter, Advanced Microwave Sounding Unit (AMSU) measurements from the National Oceanic and Atmospheric Administration (NOAA) satellite *NOAA-16* were used in the assimilation; as will be seen later, this had a detrimental effect on these stratospheric temperature analyses.

While several of the datasets are available four-times daily, for consistency the diagnostics shown here are calculated using 1200 UTC data from each product. The examination of higher- and lower-resolution versions of ECMWF and GEOS-4 products provides some insight into resolution effects.

Potential vorticity (PV) is calculated from each dataset using the same algorithm (Newman et al. 1989; Manney et al. 1996), adapted to run at higher resolution for the GEOS-4P, GEOS-4, and ECMWF-R data. GEOS-4 and ECMWF also have available PV calculated internally in the assimilation system; comparisons indicate that most of the differences noted here result from underlying differences in the analyses (and, in the case of ECMWF, from the reduced resolution of the fields used for the offline calculations), rather than differences in the PV calculation. Several diagnostics shown are based on trajectory calculations, which are done isentropically using the trajectory code described by Manney et al. (1994b). Eliassen–Palm (EP) fluxes are calculated as described by Sabutis (1997), after the datasets are interpolated to a common horizontal and vertical grid. When a common vertical grid is needed, the datasets are interpolated linearly in log(p) to the *Upper Atmosphere Research Satellite* (*UARS*) pressure levels on which the MetO data are provided, comprising six levels per decade in pressure, equally spaced in log(p). Radiosonde data compared to the analyses here were made available by the Global Telecommunication System of the World Meteorological Organization (WMO), as described by Krüger et al. (2005); radiosonde temperature observations at the South Pole are augmented by observations from the South Pole Ozonesonde Program.

3. Overview of large-scale evolution

Randel et al. (2004) compared climatological aspects of middle-atmosphere zonal mean temperatures and winds from several analyses. Here we are primarily interested in comparisons of day-to-day evolution during one particular winter. An overview of the structure and evolution of temperatures, winds, and wave diagnostics gives us a first-order picture of fundamental areas of agreement or disagreement between the analyses.

a. Temperatures

Radiosonde temperatures are commonly used in validation studies and forecast verification. Simmons et al. (2005) showed good agreement between temperature changes related to vortex evolution in radiosonde observations and ECMWF analyses and forecasts. Though radiosonde observations are used as inputs in each of the analyses, none of the assimilation systems gives high weight to the SH radiosondes; thus, these comparisons provide significant information on how well the analyses capture the detailed local temperature evolution. Figure 1 shows temperatures at 20 and 50 hPa from observations at three representative radiosonde stations in the Antarctic during August through October 2002, along with temperature differences between these and the meteorological analyses interpolated [bilinearly in latitude and longitude, linearly in log(p) in the vertical, linearly in time] to those locations. (REAN and ECMWF-R datasets, not shown, give nearly identical results to REAN-2 and ECMWF, respectively.) The major warming can be readily identified in the Amundsen-Scott and Neumayer temperatures as a sudden increase beginning around 20 September (day 50); an earlier strong minor warming is apparent at Neumayer around 8 September (day 38), and minor warmings in August are seen at Syowa. At 50 hPa, all of the analyses follow the radiosondes closely, with differences typically less than 3 K; however, the REAN-2 analysis underestimates the peak of the major warming by ~5 K at Amundsen-Scott. At 20 hPa, MetO, NCEP/CPC, and REAN-2 temperatures show an abrupt decrease with respect to the Amundsen-Scott radiosonde during the sharp temperature rise, suggesting a mismatch in the timing of that rise. REAN-2 and NCEP/CPC 20-hPa temperatures are higher than those in radiosondes and the other analyses during the cold periods in August and early September, and lower than radiosondes at Amundsen-Scott and Neumayer in the warm conditions following the major

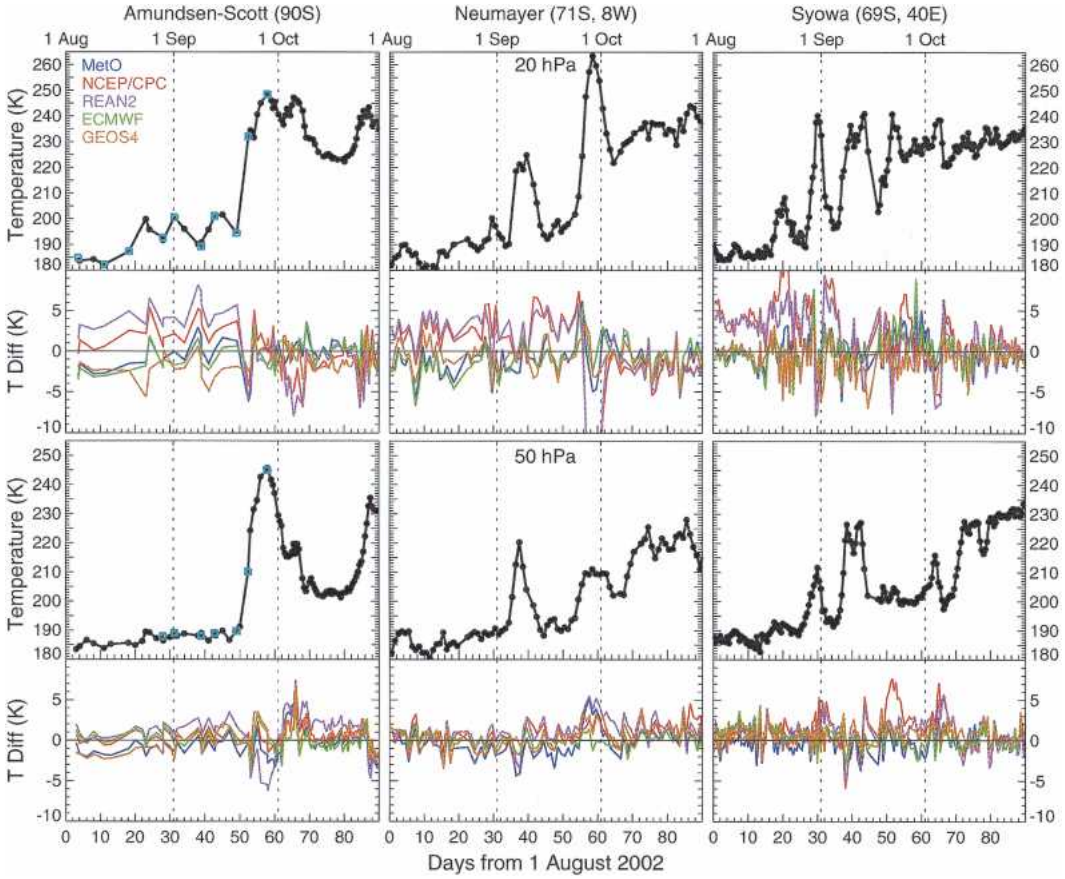

FIG. 1. Time series from 1 Aug through 31 Oct 2002 at 3 radiosonde stations. Shown are observation at 20 hPa (top row), and analysis-minus-radiosonde (second row). Similar sets are shown for 50 hPa in lower two rows. Note that black dots are from regular observations and cyan square are from the South Pole Ozonesonde Program.

warming, typically by 3–7 K; at the peak of the warming at Neumayer, REAN-2 and NCEP/CPC temperatures are both ~20 K below the radiosonde. Differences between REAN-2 and the other datasets that may account for this behavior include the lower model resolution and fewer levels in the stratosphere and the assimilation of retrieved temperatures rather than radiances. In the NCEP/CPC analyses, the interpolation to the 65 × 65 polar stereographic grid (which substantially degrades the resolution at high latitudes) may result in the lower peak temperatures. At 10 hPa (not shown), the MetO analyses overshoot the maximum temperatures seen in the radiosonde data during minor warmings in August and early September.

Similar differences between analyses are apparent for fixed points removed from radiosonde stations (not shown), with weaker extrema above 50 hPa in REAN-2 and NCEP/CPC than in the other analyses, and higher maxima in MetO analyses at 10 hPa. Figure 2 shows minimum and maximum temperatures poleward of 40°S at 50, 30, and 10 hPa during the SH 2002 winter for operational ECMWF data, and the differences between ECMWF and the other analyses, including ERA-40. Although the maxima are often near the equatorward edge of the domain (40°S) in earlier months, after early August they are always at high latitudes (poleward of ~55°S). Both minimum and maximum temperatures agree well at 50 hPa, with differences typically less than 3 K; the exceptions are very low ERA-40 minimum temperatures in August and an underestimate of several maxima in REAN-2 after mid-August, when dynamical activity increased. Maximum temperatures generally agree at 30 hPa, but REAN-2 shows larger underestimates of the maxima; 30 hPa minimum ERA-40 and REAN-2 temperatures are higher than those in the other analyses by 3–8 K. A larger spread among the analyses is seen at 10 hPa, commonly as much as ~10 K, with REAN-2 and NCEP/CPC showing lower maximum temperatures; ECMWF, MetO, and NCEP/CPC minimum temperatures are similar, with REAN-2 and ERA-40 higher and GEOS-4 lower by 3–10 K. Note that ERA-40 minimum temperatures are biased high at 10 and 30 hPa from May through August, but slightly low at 50 hPa; the shift from low to high bias is indicative of the vertically oscillatory Antarctic temperature structure reported by Randel et al. (2004) and Sim-

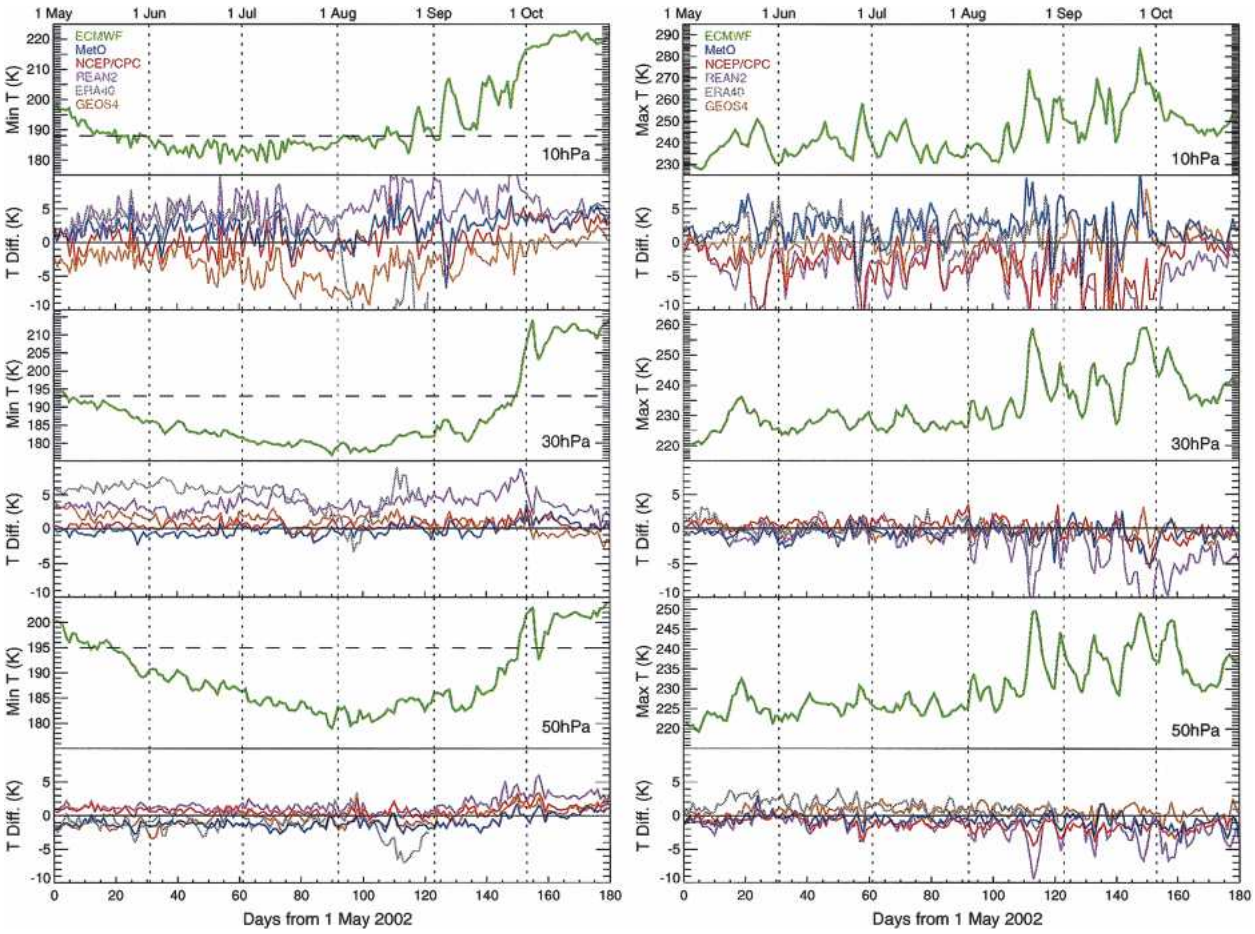

FIG. 2. (left) Minimum and (right) maximum temperatures poleward of 40°S at (top) 10, (middle) 30, and (bottom) 50 hPa during the 2002 Antarctic winter, from ECMWF, and (multicolor) differences between them and those from the NCEP/CPC, REAN-2, ERA-40, and GEOS-4 analyses. Differences are analysis − ECMWF, so negative values indicate that the other analysis is colder than ECMWF. The dashed horizontal lines in the ECMWF minimum temperature panels show the approximate NAT PSC formation threshold at each level.

mons et al. (2005). Also, as noted above, differing inputs into ERA-40 in August 2002 resulted in further degradation of the stratospheric temperature structure, as seen in very low minimum ERA-40 temperatures at 10 and 50 hPa, and high minimum temperatures at 30 hPa.

Figure 3 shows time–pressure cross sections of 60°S zonal mean temperature from ECMWF and differences between ECMWF and the other datasets. The unrealistic ERA-40 temperature structure in August is readily apparent, and higher temperatures near 50–10 hPa result from the vertical oscillations in temperature. Because of these artifacts, the ERA-40 temperatures are not recommended for detailed analyses of temperatures evolution in the 2002 SH winter. ECMWF, MetO, NCEP/CPC, and GEOS-4 after early August show small differences, less than 3 K, below 10 hPa, with slightly larger differences in REAN-2. GEOS-4 shows a band of significantly lower temperatures between 30 and 10 hPa before early August. The development of and recovery from the major warming show good agreement among the analyses. Larger differences are seen above ~5 hPa, where MetO, NCEP/CPC, and GEOS-4 are all substantially higher (2–8 K) than ECMWF, though these analyses generally (excepting MetO in July) come back into better agreement near 1 hPa. Larger differences in the upper stratosphere are expected, since Television Infrared Observation Satellite (TIROS) Operational Vertical Sounder (TOVS) satellite soundings (used in all the analyses) stop at 1–2 hPa and provide only about three pieces of information for a layer over 20 km thick (e.g., Li et al. 2004, manuscript submitted to *J. Atmos. Sci.*, hereafter LPBL); thus the analyses are more sensitive to underlying model differences at higher altitudes.

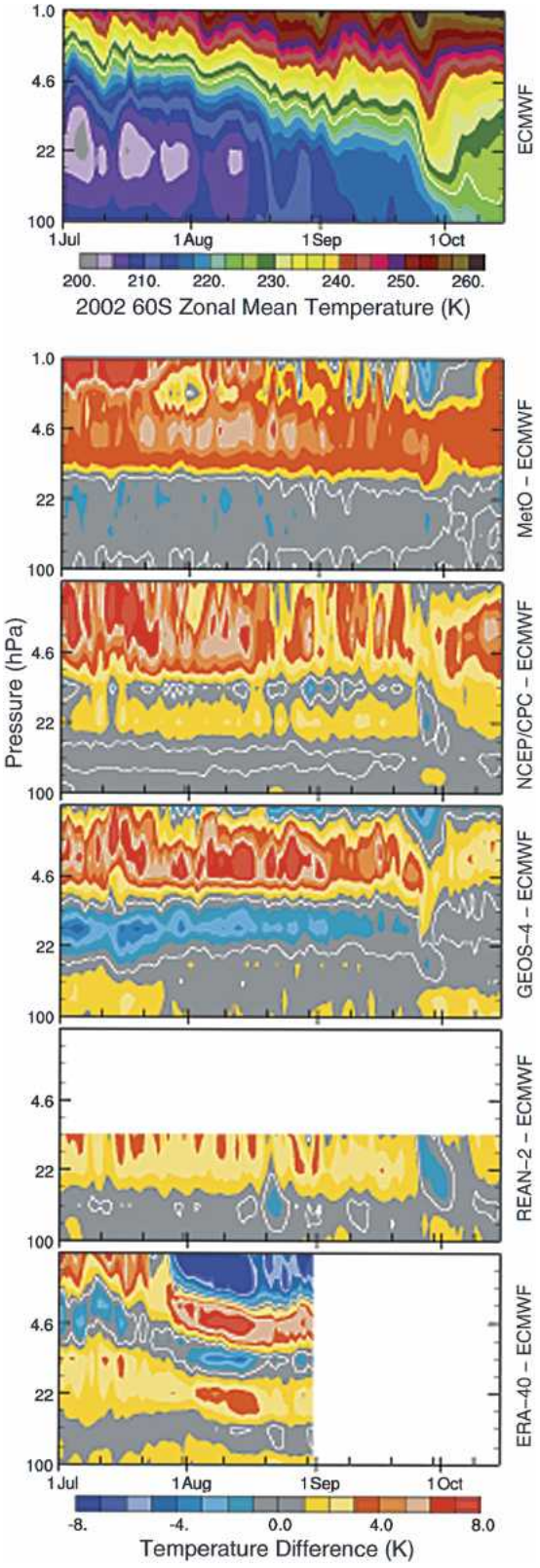

b. *Winds and wave diagnostics*

High-latitude zonal mean winds from all analyses agree very well below 10 hPa; Manney et al. (2005) show the 10-hPa wind reversal on 25 September and return to westerlies on 30 September in MetO, NCEP/CPC, ECMWF, and GEOS-4 analyses, indicating that zonal mean winds typically agree within 1–3 m s^{-1} during September–October. However, as shown in Fig. 4, REAN-2 gives weaker westerlies prior to, and weaker easterlies near 70°S during, the major warming by up to ~6–10 m s^{-1} at 10 hPa. ERA-40 zonal mean winds are consistent with those in other analyses (Fig. 4 shows differences typically less than 3 m s^{-1} south of 50°S) despite the unrealistic temperature structure (section 3a) because the temperature anomaly is oscillatory (so the wind shear related to it integrates to near zero in the vertical) and of broad horizontal scale (so the meridional temperature derivative related to it is small). Larger differences are apparent in upper-stratospheric winds (not shown), as may be expected from weaker data constraints in the assimilation systems in this region (e.g., LPBL). Gray et al. (2003) discuss some differences, largest in the upper stratosphere, between MetO, ECMWF, and ERA-40 equatorial winds; GEOS-4 equatorial winds are more similar to the ECMWF and ERA-40 products shown by Gray et al. (2003), with westerlies related to the semiannual oscillation extending down to ~2 hPa.

Diagnostics of wave propagation are important to many dynamical studies (e.g., Krüger et al. 2005; Harnik et al. 2005; Newman and Nash 2005; Scaife et al. 2005). Figure 5 shows the ECMWF EP flux divergence at 22 hPa (the highest level where calculations from REAN are reliable) and 68°S (the latitude where the largest fluxes are observed) and the vertical EP flux component at 100 hPa at 60°S (latitude of largest values) during August through October, along with differences between ECMWF and the other analyses. The vertical component at 100 hPa, representing the upward propagation in the lower stratosphere, is very similar in all the analyses, with differences up to ~15%; MetO and GEOS-4 often show lower values than the other analyses, including at the time of the large upward wave pulse that triggered the major warming. As shown by Manney et al. (2005), quite small differences in the vertical EP flux component may result in large differences in propagation through the stratosphere. Eliassen–Palm flux divergences also show generally good agreement, but at 22 hPa the magnitudes are often smaller in the REAN calculations by up to about 25%.

←

FIG. 3. (top) Zonal mean temperature (K) at 60°S as a function of pressure and time from ECMWF, and differences between ECMWF and (second to bottom panels, respectively) MetO, NCEP/CPC, GEOS-4, REAN-2, and ERA-40, for Jul–Oct 2002 (ERA-40 only through Aug). Differences are analysis − ECMWF, so negative values indicate that the other analysis is colder.

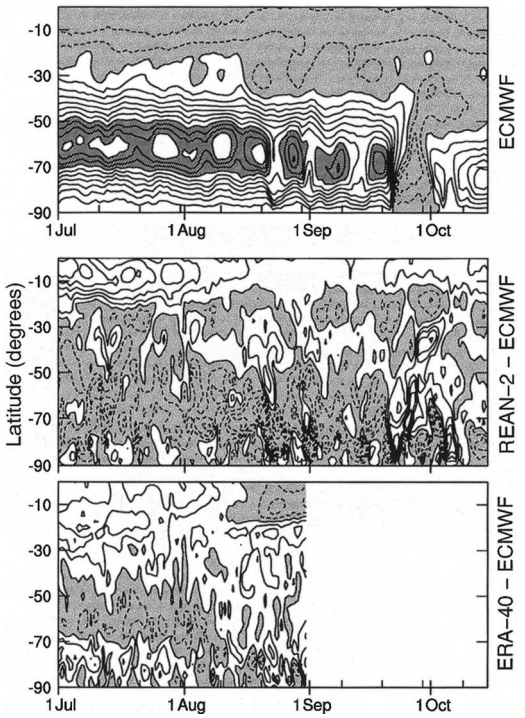

FIG. 4. (top) The 10-hPa zonal mean winds (m s^{-1}) as a function of latitude and time from ECMWF, and (other panels) the differences between ECMWF and REAN-2 and ERA-40, for Jul–Oct 2002 (ERA-40 only through Aug). Contour interval for ECMWF is 10 m s^{-1}, with light shading for values less than zero and dark shading from 70 to 90 m s^{-1}. Contour interval for differences is 2 m s^{-1}, with values less than zero shaded. Differences are analysis − ECMWF, so negative values indicate weaker westerlies or stronger easterlies.

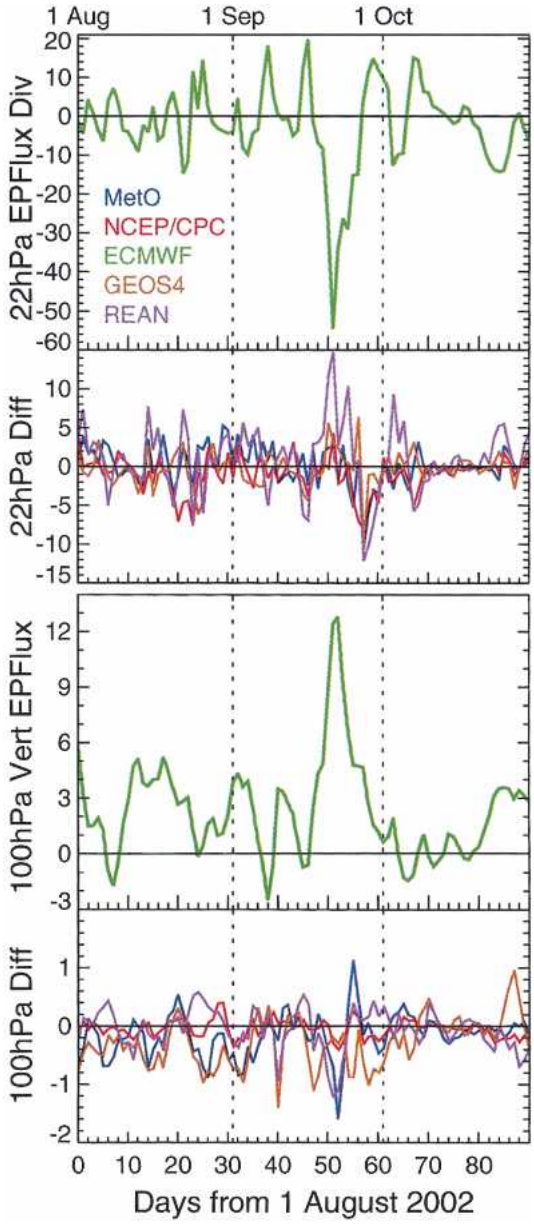

FIG. 5. (top) EP flux divergence (expressed as wave driving, m s^{-1} day^{-1}) at 68°S and 22 hPa and (third from top panel) vertical EP flux component (10^{12} m s^{-2}) at 60°S and 100 hPa, for Aug–Oct 2002 in the SH, for ECMWF. (other two panels) Difference between ECMWF and the other analyses. Differences are analysis − ECMWF, so negative values indicate lower (more negative or less positive) values in the other analysis.

These broad comparisons show overall agreement between MetO, ECMWF, and GEOS-4 temperature structure and evolution in the lower to middle stratosphere, with large differences between all analyses in the upper stratosphere. NCEP/CPC fields often underestimate temperature extrema, and ERA-40 and REAN-2 temperatures should be used, at best, with great caution for detailed studies of the 2002 SH winter. Winds and wave propagation diagnostics throughout the winter give a consistent picture from all the analyses, but some caution is warranted in using REAN/REAN-2 winds or EP fluxes for detailed studies in the top few levels (between about 30 and 10 hPa) for which they are available. In the following sections, we turn to more detailed comparisons of fields and diagnostics used in scientific studies.

4. Synoptic structure and evolution during the major warming

Several studies have focused on synoptic evolution during the major warming (e.g., Krüger et al. 2005; Manney et al. 2005; Simmons et al. 2005), including the day-to-day evolution of winds, PV, and other fields. In these comparisons of meteorological analyses, many aspects of the synoptic evolution have been found to agree quite well among analyses, including the day-to-day evolution of temperatures and winds and their 3D structure. For instance, all of the operational analyses (ECMWF, NCEP/CPC, MetO, GEOS-4) show very good quantitative agreement in the temperature evolu-

tion through the middle stratosphere and qualitative agreement through the upper stratosphere, especially in the formation and evolution of "baroclinic zones" (regions of strong meridional temperature gradients with a tilted vertical structure along the edge of the vortices; e.g., Manney et al. 2005) similar to those typical during NH major warmings (e.g., Fairlie et al. 1990; Manney et al. 1994a). Other aspects of the synoptic evolution may be more dependent on which analyses are examined.

Anomalous transport during stratospheric warmings occurs in connection with enhanced vertical velocities along the baroclinic zones (e.g., Manney et al. 1994a, 2005), and often depends strongly on those velocities. Figure 6 shows cross sections of ω, the vertical velocity in pressure coordinates, from the MetO, ECMWF, and GEOS-4 operational assimilation products (NCEP/CPC objective analyses do not provide vertical velocities). The MetO and GEOS-4 ωs are from 6-h averages valid at 1200 UTC (all other MetO fields are synoptic at 1200 UTC), whereas the ECMWF ωs are snapshots at 1200 UTC (hence noisier fields); thus, meaningful comparisons are limited to overall, large-scale features. These are averaged over three days, 24–26 September, during the peak of the warming when the vortex is most strongly tilted and vertical velocities are strongest (e.g., Manney et al. 2005). All of the analyses show very similar magnitudes and patterns of strongly enhanced downward motion near 40°–140°E and ~260°–320°E, along the edges of the split vortices, with slightly stronger values near 40°–140°E in the GEOS-4 analyses. Regions of enhanced upward motion are qualitatively similar (except for the suggestion of a significant region of upward motion near 180° in ECMWF analyses), but with the GEOS-4 analyses showing higher values near 220°E. Thus, all the analyses capture the large-scale patterns of enhanced vertical velocities associated with the major warming, and the magnitudes of the vertical velocities are in reasonable agreement with each other. The good quality of the forecasts produced by ECMWF (Simmons et al. 2005) suggests that their synoptic vertical velocities must be realistic, and hence overall agreement with the other datasets indicates reasonable quality in all the synoptic vertical velocities during the major warming. However, detailed transport calculations may be influenced by some of the quantitative differences noted above.

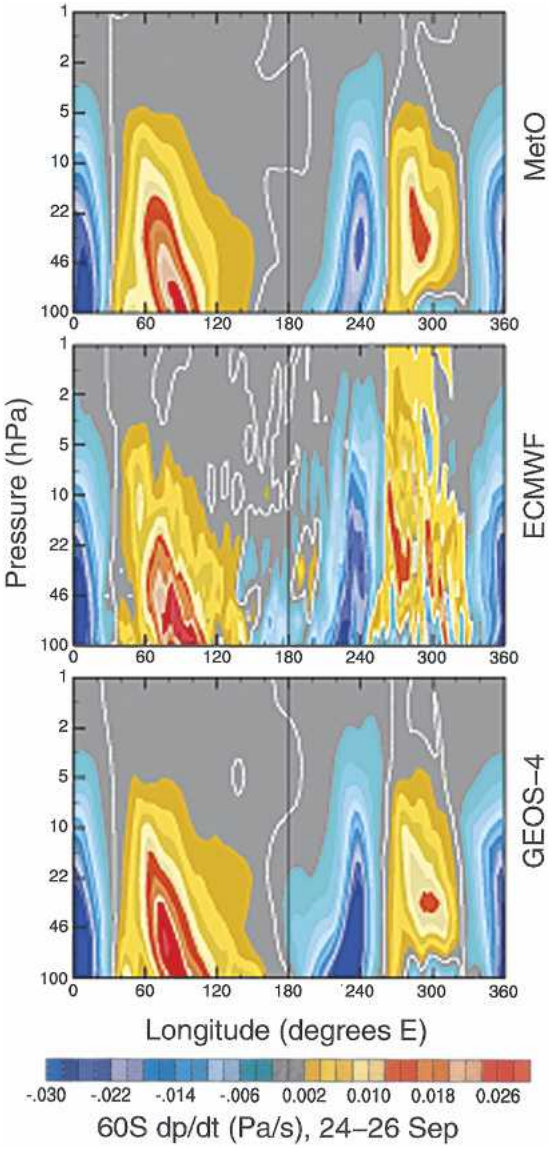

FIG. 6. Cross sections of ω (Pa s^{-1}; vertical velocity in pressure coordinates) around 60°S averaged over 24–26 Sep 2002 from (top) MetO, (middle) ECMWF, and (bottom) GEOS-4 analyses. Values provided by each data center represent different time averages, as described in the text. Positive values indicate downward motions; white contour is zero line.

Although, as shown in section 3, the mean features of the large-scale stratospheric flow are similarly represented in each of the analyses, there are often small, but potentially significant, differences in the synoptic fields and evolution. These can become particularly important in PV calculations, where differences may be magnified because PV is a highly derived field. In the middle and lower stratosphere (not shown), the differences are modest and largely quantitative. Figure 7 shows upper-stratospheric "scaled PV" (sPV, in "vorticity units"; e.g., Dunkerton and Delisi 1986; Manney et al. 1994b) from each of the analyses at 1450 K (~40–42 km) during the warming, with a few temperature contours overlaid. While the temperatures show close agreement between all analyses (with NCEP/CPC having slightly lower maxima and higher minima), much larger differences are seen between PV fields.

On 24 September the vortex is just splitting in the upper stratosphere. The NCEP/CPC and GEOS-4 analyses show more completely split vortices than the MetO and ECMWF fields. There are also significant differences in vortex strength (i.e., PV gradients across

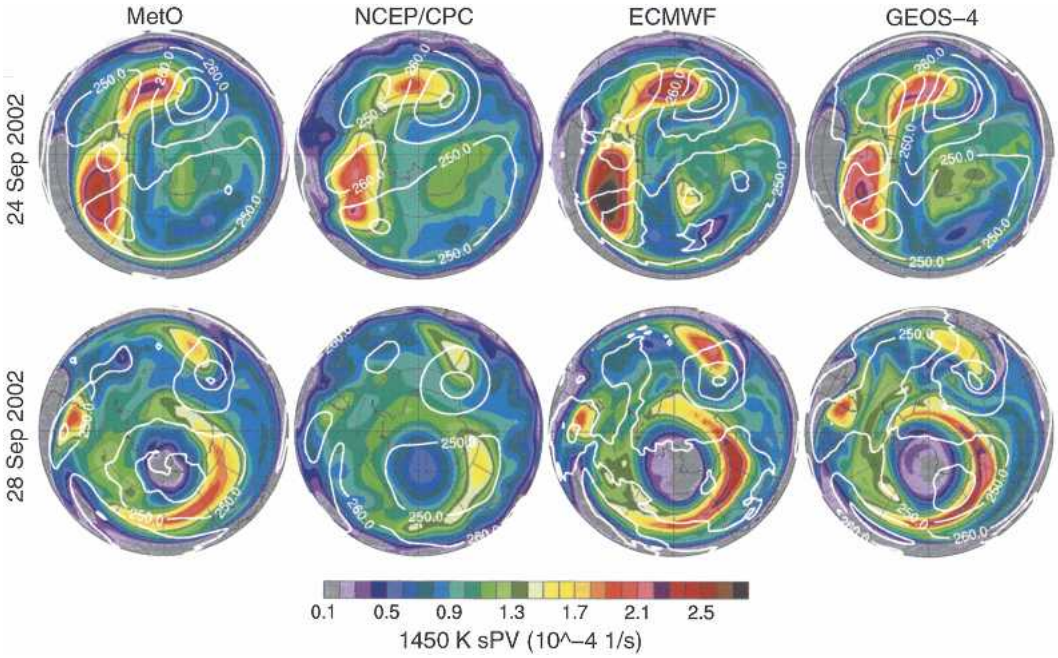

FIG. 7. The 1450-K sPV maps on 24 and 28 Sep from each of four meteorological analyses (MetO, NCEP/CPC, ECMWF, and GEOS-4). Temperature contours are overlaid in white; contour interval is 10 K. Domain is from equator to pole with dashed circles at 30° and 60°S; 0° longitude is at the top and 90°E to the right.

the vortex edge), with strongest (weakest) vortices in ECMWF (NCEP/CPC) analyses, and in the degree to which we can identify air being pulled off the larger vortex near 40°S across 180°. The higher values of PV in the 80°–160°E region south of 60° represent vortex air that has been entrained into the anticyclone; these values vary as well, and all except NCEP/CPC suggest finer-scale structure within the anticyclone region. Air being drawn up from low latitudes around the vortex and coiling into the anticyclone is suggested in all except the NCEP/CPC analyses, but is better defined in the ECMWF and GEOS-4 fields. Examination of PV calculated internally in the assimilation systems for ECMWF and GEOS-4 reveals even better definition of smaller-scale structure such as the coiled tongues of vortex and low-latitude air in the anticyclone, especially in ECMWF, for which the calculations shown here were done using reduced-resolution fields; while these internally calculated fields are preferable for scientific studies because of their internal consistency and better definition of structure in the PV fields, we show the offline calculations here to be comparable to the PV calculated for the other analyses.

On 28 September, the remnants of the upper-stratospheric vortex comprise three widely separated fragments, the largest of them coiled around a strong, confined anticyclone at high latitudes. Not only do the strength and size of the anticyclone vary (with a much weaker anticyclone in the NCEP/CPC analyses), but there are also distinct differences in the shape, strength, and position of the vortex fragments. The structure of the interwoven tongues of vortex-edge and low-latitude air is best defined in GEOS-4; however, these features are also seen in ECMWF (used at reduced resolution here) and are apparent in reduced resolution GEOS-4L fields (not shown), suggesting that we get more information from the high-resolution assimilation systems, even when we are using a reduced-resolution version of those fields. Examination of high-resolution ECMWF PV fields indicates coherent small-scale structure better defined than that in GEOS-4, which in turn shows better definition of this structure in the internally calculated PV fields.

Compared to the analyses from assimilation systems, PV from the NCEP/CPC objective analyses shows weaker vortices and anticyclones and fails to capture the filamentary and tonguelike structure suggested in the other analyses. This difference probably results largely from the assimilation-based wind fields used to calculate PV being refined by information from the underlying GCMs beyond what may be derived directly from the increasingly sparse data at these levels (in contrast to the NCEP/CPC, which uses balanced winds derived from geopotential heights); the models' input to defining the vertical temperature gradients involved in the calculation may also play a role, although we suggest that this is less important since examination of temperature cross sections (not shown) indicates structure and gradients in the upper-stratospheric NCEP/CPC fields very similar to that in other analyses.

Differences in PV such as those shown here may be important in many studies, including defining the level

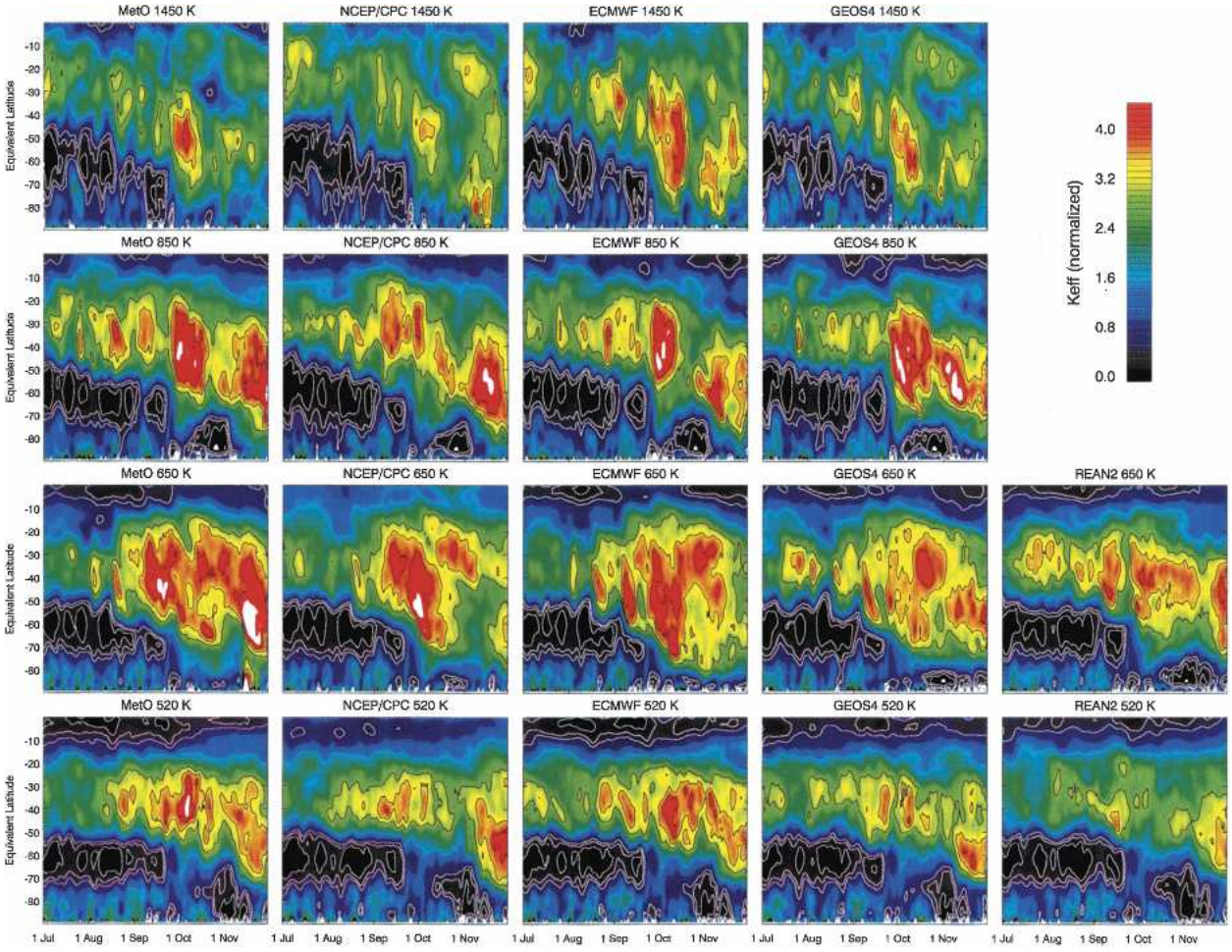

FIG. 8. Effective diffusivity, K_{eff}, expressed as log-normalized equivalent length, at (top to bottom) 1450, 850, 650, and 520 K in the SH late winter and spring (Jul–Nov) 2002, calculated using the model of Allen and Nakamura (2001) from (left to right) five meteorological datasets. REAN-2 analyses are not shown at 850 and 1450 K since they do not extend through these levels.

of detail to which we can understand the 3D structure and evolution of the polar vortex. Such differences in detail are also fundamental to understanding the accuracy and reliability of products derived from correlations of trace gases with PV, such as the proxy ozone of Randall et al. (2005), which relies on fitting sparse solar occultation data against PV to reconstruct synoptic fields.

5. Mixing, transport barriers, and finescale structure

During the 2002 SH winter, unusually strong wave activity led to greatly enhanced quasi-isentropic transport and mixing, including small-scale mixing with extensive filamentation of material pulled off the vortex (e.g., Allen et al. 2003; *JAS*). Models and observations of ozone and other trace gases indicated strongly enhanced poleward transport and mixing dominating the trace-gas evolution over the period of the major warming (e.g., Manney et al. 2005; Randall et al. 2005; Siegmund et al. 2005). Konopka et al. (2005) and Marchand et al. (2005) used high-resolution calculations driven with ECMWF winds to quantify transport and mixing of vortex air into midlatitudes. In the following, we examine the representation of these processes in each of the meteorological analyses.

a. Diagnostics of mixing and transport barriers

Figure 8 shows effective diffusivity (K_{eff}, expressed as log-normalized equivalent length) calculated as described by Allen and Nakamura (2001, 2003); an idealized tracer was initialized on 1 April 2002 with the tracer equivalent latitude from Allen and Nakamura (2003) and advected isentropically until November using winds from each of the analyses. Effective diffusivity K_{eff} provides a measure of mixing and transport barriers (e.g., Haynes and Shuckburgh 2000a,b; Allen and Nakamura 2001; Tan et al. 2004), with low values

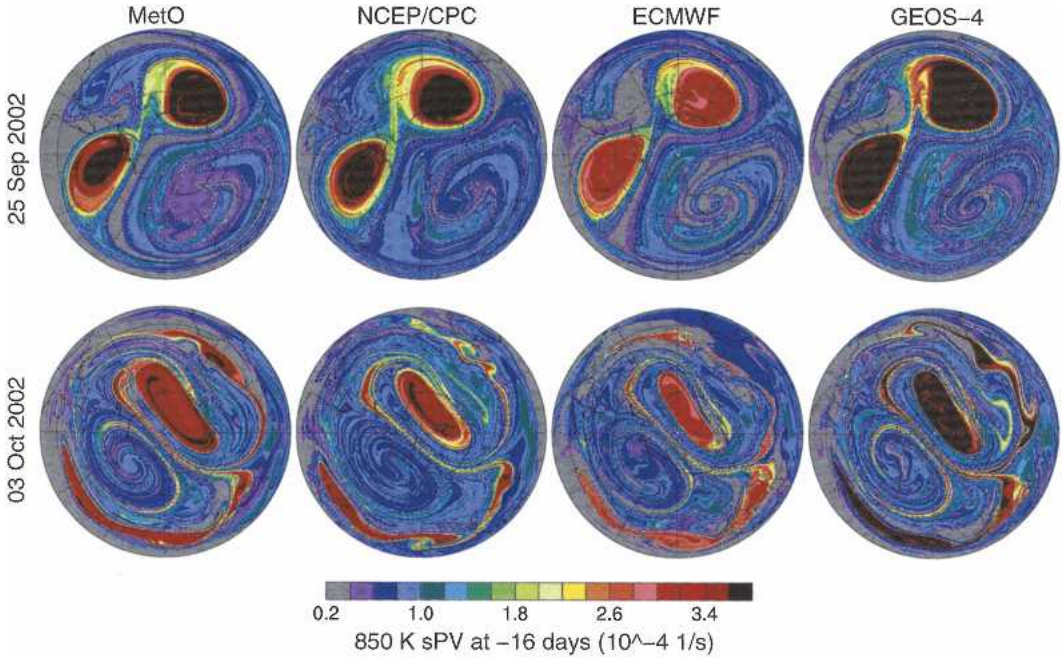

FIG. 9. The 850-K "PV tracer" maps on (top) 25 Sep and (bottom) 3 Oct 2002 from high-resolution isentropic trajectory calculations using each of four meteorological analyses. Back trajectories are initialized with sPV 16 days before date shown. Layout is as in Fig. 7.

representing transport barriers and high values representing strong mixing.

The lack of a strong transport barrier in NCEP/CPC calculations in the equatorial lower stratosphere arises primarily from the use of balanced winds. GEOS-4 and REAN-2 also show weaker subtropical barriers than MetO and ECMWF in the lower stratosphere (650 and 520 K). Previous studies (e.g., Rogers et al. 1999; Douglass et al. 2003; Schoeberl et al. 2003; Tan et al. 2004) have shown that assimilated or analyzed datasets give an excess of subtropical transport; thus, we expect that the analyses with stronger transport barriers (less subtropical transport) are more realistic. The polar vortex transport barrier is similar in all analyses, except at 650 K, where the REAN-2 vortex is slightly stronger immediately before, decays less completely during, and recovers more fully after, the major warming than that in the other analyses; the 650-K GEOS-4 vortex also recovers more strongly than that in MetO, NCEP/CPC, and ECMWF.

The MetO and ECMWF calculations typically show most mixing during and immediately following the major warming, while REAN-2 shows much less mixing at 520 K than the other analyses in that time period. The patterns of mixing in November, as the final warming occurs, show large differences in the middle to lower stratosphere: much stronger mixing is seen in NCEP/CPC at 520 K, in MetO and REAN-2 at 650 K, and in MetO and NCEP/CPC at 850 K; thus, quite different vertical structures of mixing during the final warming among the analyses are indicated. Overall, maximum midlatitude K_{eff} values at 1450 K are comparable in MetO, ECMWF, and GEOS-4, but 15%–20% lower in NCEP/CPC; at 850 K, all maximum mixing values are within 10% of each other, with highest values in GEOS-4. In the lower stratosphere there is more scatter in maximum values, but REAN-2 has lowest values (by 10%–20%) at both 650 and 520 K. Although most of these differences in magnitude are modest, they are accompanied by differences in timing, location, and duration of maximum mixing. The time of maximum mixing at 1450 K is similar in each analysis, but magnitudes and spatial extent vary considerably; at each of the other levels, there is not even agreement on the timing of strongest mixing. Thus, there is little consensus on the amount, patterns, or timing of mixing in midlatitudes, nor on the extent of mixing into the polar regions during the major warming. Such variations in mixing between analyses are expected to result in significant differences in transport calculations driven with different analyses.

b. Filamentation

To examine how differences in mixing are manifested in synoptic fields, we show maps of a high-resolution "PV tracer" at 850 K (Fig. 9) during the major warming. Isentropic reverse trajectory (RT) calculations (e.g., Manney et al. 1998, 2000, and references therein) were initialized with sPV. The differences in the magnitude of PV-tracer values between analyses result primarily from differences in the sPV fields used for initialization, but examination of fields initialized with ECMWF data

for each analysis (not shown) indicates that all the other differences discussed below arise primarily from differences in transport using winds from the various analyses. Quite significant differences are seen in the size and strength of the vortex. For instance, a stronger (i.e., larger PV gradients along the edge) and deeper (i.e., higher PV values within) vortex is seen in GEOS-4 analyses, and a smaller and weaker vortex in ECMWF analyses (especially on 25 September). Substantial differences are seen in material pulled off the vortex and entrained into the anticyclone: higher-valued vortex filaments in the anticyclone (90°–120°E, 50°–70°S on 25 September; 180°–270°E, 40°–80°S on 3 October) in the GEOS-4 calculations and differences in the position and size of the 3 October filament near 40°S in the 0°–90°E sector. Differences in material pulled up from low latitudes include larger tongues of low values around the vortex edge and in the anticyclone in ECMWF and MetO on 25 September, and less low-latitude air pulled up around the vortex regions in all NCEP/CPC calculations compared to those driven with the other analyses (resulting from the use of balanced winds). Differences in local vortex strength (e.g., variations in vortex edge gradients near 330°–360°E and between the two vortices on 25 September) could result in different conclusions about the amount of entrainment of material into the vortex. Differences are of similar character at lower levels. REAN-2 calculations in the lower stratosphere (not shown) give a weaker and shallower vortex and show less filamentary structure outside the vortex.

The GEOS-4 calculations show more complex fine-scale structures outside the vortex than the calculations with the other analyses (especially at lower levels). Comparison with calculations using GEOS-4L data, which were interpolated from 1° × 1.25° to 2° × 2.5° (not shown; and of 2.5° × 2.5°ECMWF with 1.25° × 1.25° ECMWF-R results), indicates that only a small part of this arises from using the analysis at higher resolution.

c. *Lamination in trace gas profiles*

Grooß et al. (2005) and Konopka et al. (2005) show examples where chemical transport model (CTM) calculations driven with ECMWF data reproduced filaments in Halogen Occultation Experiment on *UARS* (HALOE) data. We examine filamentation quantitatively here using RT calculations to model small vertical-scale laminae in ozone (e.g., Manney et al. 1998, 2000, and references therein). Figure 10 shows two Stratospheric Aerosol and Gas Experiment (SAGE) III ozone profiles with laminar structure in the lower stratosphere observed at different times and longitudes on 23 September—the first with a local maximum (minimum) near 480 (540) K, and the second with a local maximum (minimum) near 490 (525) K. Ten-day reverse-trajectory calculations for these profile locations using ECMWF, MetO, NCEP/CPC, and GEOS-4

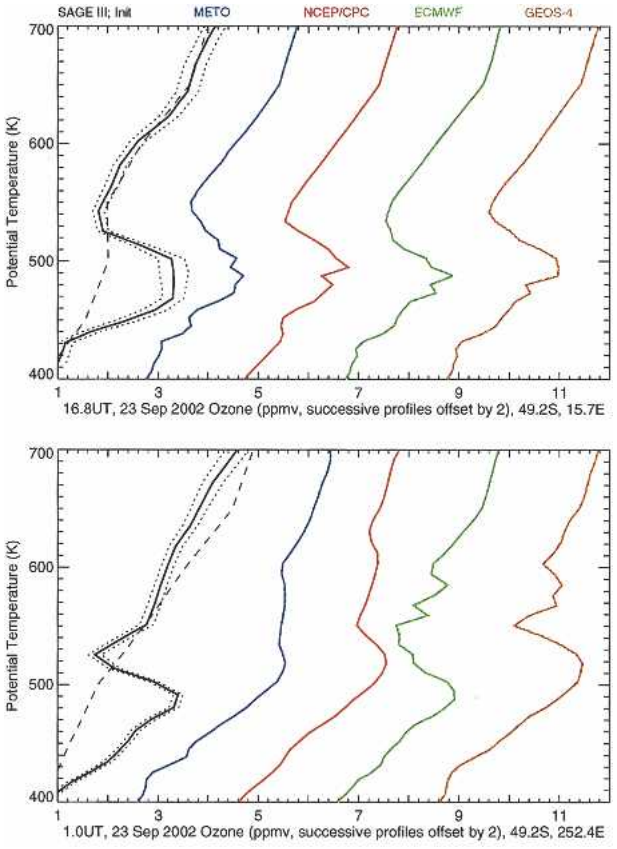

FIG. 10. Two SAGE III ozone profiles (thick black curves, with estimated random error as dotted lines) and profiles from high-resolution RT calculations using each of four different meteorological analyses (colors). Dashed black line with SAGE profiles shows the profiles at the SAGE III locations from the initialization fields.

winds were initialized with "proxy" ozone based on reconstructing 3D fields using ozone/PV correlations for SAGE III, HALOE, and Polar Ozone and Aerosol Measurement (POAM) III data (Randall et al. 2005). The dashed black lines show the proxy ozone used for initialization at the SAGE III observation locations. For the first profile, there is a greatly smoothed echo of the lamina pair in the initialization field (suggesting that there is some indication of this feature in the PV field), while for the second profile, the proxy field shows no evidence of the lamina pair (suggesting that this feature in ozone does not arise from something that is represented in the PV fields used for proxy reconstruction).

Calculations from all analyses show a similar maximum/minimum pair for the first profile. There are noticeable differences in the calculations of very small scale structure for this profile, but since these very small scale structures are not represented in the SAGE III profile, we have no way to judge whether one might be more realistic than another. Examination of RT ozone maps (not shown) indicates that this lamina pair arises

from the observations crossing the edge of the tilted vortex at those levels; RT calculations have previously been found to be most successful at refinement of the representation of gradients along the vortex edge (e.g., Fairlie et al. 1997; Manney et al. 1998), so it is not too surprising that the analyses do well in this case. However, the assimilated fields do better than NCEP/CPC (where balanced winds are used) at capturing the shape of the minimum near 430 K, and ECMWF does better than the other analyses at capturing the shape of the minimum near 525 K. In contrast, the lamina pair in the second profile arises from sampling a very narrow filament of lower-ozone (lower latitude) air drawn into the collar region of high ozone along the vortex edge, a situation where detailed simulation is much more difficult (e.g., Manney et al. 1998). None of the calculations reproduce this feature, but there is large variation in the degree to which the calculations capture any indication of the observed profile. The MetO calculations show little suggestion of a minimum corresponding to that in the SAGE profile, and the NCEP/CPC calculations show only a hint of a minimum near 560 K. The ECMWF analyses and GEOS-4 calculations each show a maximum/minimum pair, but located a bit higher than in SAGE (near 490/540 K for ECMWF and 510/550 K for GEOS-4). The MetO analyses, which do very poorly, had at this time the poorest vertical resolution in the lower stratosphere; the better (though still imperfect) performance of GEOS-4 and ECMWF may be related to the better vertical resolution of these assimilation systems in the lower stratosphere (see Table 1, and references therein).

The above diagnostics reveal considerable discrepancies between the analyses in timing, location, and magnitude of enhanced transport and mixing, though representation of the polar vortex transport barrier is reasonably consistent. Our calculations of the development of finescale structure show that some of these interanalysis variations are related to differences in the development and evolution of filaments and the interweaving of narrow tongues of low latitude and vortex air. Development of more filamentary structure and better simulations of laminae in ECMWF and GEOS-4 analyses suggests (as was the case for the PV fields shown in section 4b) a benefit from higher-resolution assimilation systems, even when their results are used at reduced resolution. The relatively large differences in small-scale structure and mixing imply that significant differences would be expected in more detailed transport calculations. Such differences could be important to studies like those of Grooß et al. (2005), Konopka et al. (2005), and Marchand et al. (2005), which rely on quantitative modeling of filaments and vortex fragments.

6. Polar processing diagnostics

Model studies of polar chemical processing and ozone loss in the lower stratosphere, including several of the 2002 SH winter (e.g., Sinnhuber et al. 2003; Feng et al. 2005; Grooß et al. 2005; Marchand et al. 2005), depend strongly on temperatures and temperature histories. Figure 11 shows the area in which temperatures are low enough for nitric acid trihydrate (NAT) polar stratospheric cloud (PSC) formation as a function of time and pressure for ECMWF and the differences between ECMWF and each of the other analyses. [The criterion of Hanson and Mauersberger (1988) is used, with HNO_3 and H_2O values from UARS profiles as described by Manney et al. (2003).] Differences between ECMWF, MetO, and NCEP/CPC are small (usually less than 1% of a hemisphere, or up to a 10% variation among analyses), as are GEOS-4 differences below about 20 hPa; above 20 hPa, GEOS-4 shows a substantial cold bias compared to ECMWF (up to ~6% of a hemisphere). The radiosonde comparisons discussed in section 3a show closer agreement with MetO, ECMWF, and NCEP/CPC at these levels.

The REAN-2 and ERA-40 reanalyses are included to highlight the problems in their lower-stratospheric temperature fields. REAN-2 temperatures are biased high with respect to the other analyses by as much as ~7% of a hemisphere (over a 50% bias) between ~60 and 10 hPa; this bias is large enough to have a substantial effect on polar processing studies. The oscillatory vertical structure in ERA-40 temperatures results in a much smaller cold region between about 50 and 20 hPa than the other analyses, and the unrealistic temperature structure in August is obvious in the large cold area near 10 hPa.

Because the SH winter is so cold, with a large fraction of the vortex having temperatures well below both NAT and ice PSC formation thresholds for several months, even the 3–6-K biases seen above between analyses might be expected to result in only small percentage changes in calculations of, for example, denitrification or ozone loss. As noted by Pawson et al. (1999) for the NH, temperature differences are most likely to have a significant effect on polar processing studies when conditions are marginal for PSC existence, namely in fall or spring in the SH, when the timing of the onset or disappearance of PSCs may vary and may affect such studies.

To examine the likelihood and timing of PSC formation in spring and fall, we performed temperature history calculations like those of Manney et al. (2003), with starting dates a few days after the onset of $T \leq T_{NAT}$ in fall (May) and a few days before the disappearance of $T \leq T_{NAT}$ in spring (in this case, earlier than usual, in September during the major warming). The T_{NAT} values at 465 and 585 K are taken to be 195 and 193 K, respectively [approximate values from Hanson and Mauersberger (1988)]. Parcels were initialized on a dense equal area grid within the region with $T \leq T_{NAT}$ and were run 20 days back and 20 days forward using winds from each of the analyses. As in Man-

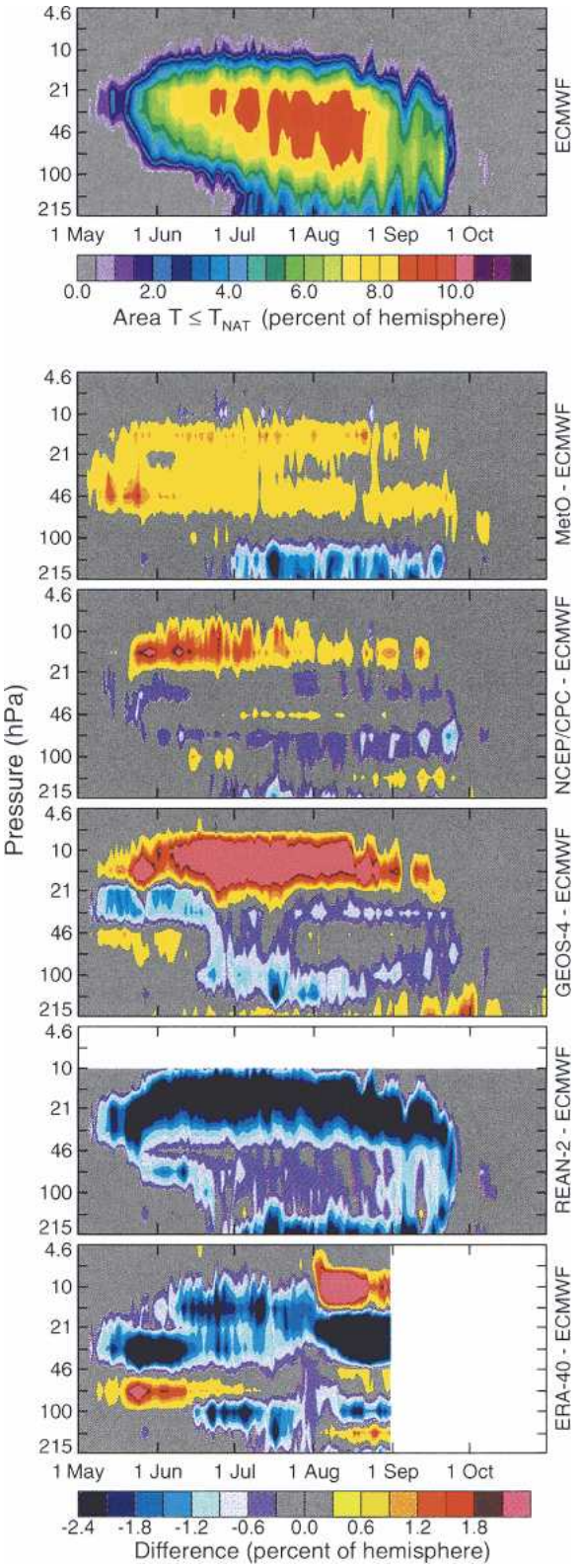

ney et al. (2003) we calculate the total number of days that each parcel was at or below T_{NAT} (Fig. 12) and the continuous time before and after the initialization date that each of the parcels remained below T_{NAT} (Fig. 13). The latter diagnostic is related to PSC duration and denitrification and can be viewed as an idealized or potential PSC lifetime. The former, giving an indication of the total time when PSCs are present, is related to chlorine activation. At 465 K, there is fair agreement in overall distributions between the analyses in total PSC days (Fig. 12), but MetO, and to a lesser degree GEOS-4, analyses for 26 May show stronger peaks at a larger number of days (around 25 and 21 days for MetO and GEOS-4, respectively), and REAN-2 analyses show a strong peak near 13–14 days that is absent in the other analyses. At 585 K, the REAN-2 analysis stands out as an outlier, with strong peaks near 11 and 20 days for 26 May, as opposed to ~23 days for NCEP/CPC, and ~26–31 days for the other analyses. For 13 September, REAN-2 shows a compact distribution contained from 1 to 7 days, as opposed to broad distributions extending to 22–27 days for the other analyses. Despite the broad qualitative resemblance between MetO, ECMWF, and GEOS-4 distributions at both levels, even among these there are significant differences in detail that might be expected to affect quantitative polar processing studies. The PSC lifetime distributions (Fig. 13) also show significant variations among all analyses, especially in the existence of peaks at longer lifetimes [e.g., over 20 days in MetO, GEOS-4, and REAN-2 in May, and in MetO and (weakly) ECMWF in September]. The existence or lack thereof of PSCs with such long lifetimes could have important implications for denitrification.

Overall, PSC formation potential and temperature histories in the SH 2002 winter exhibit much better agreement than is typical during the NH winter (Manney et al. 2003); however, there are still differences among all analyses significant enough to affect the results of polar processing studies. The REAN/REAN-2 results again argue against using these analyses for detailed polar processing studies in the SH.

7. Summary and conclusions

Most studies of the unique SH 2002 winter rely on gridded meteorological data from one of several commonly used analysis systems, and the dataset used can influence the results. We have compared diagnostics related to temperature evolution and lower-strato-

←

FIG. 11. Pressure–time cross sections of the area with $T \leq T_{NAT}$ (percent of a hemisphere) for May–Oct 2002 in the SH from (top) ECMWF, and the differences between ECMWF and (top to bottom) MetO, NCEP/CPC, GEOS-4, REAN-2, and ERA-40 (through Aug). Red–oranges–browns indicate a larger cold region (associated with lower temperatures) in the analysis being compared to ECMWF.

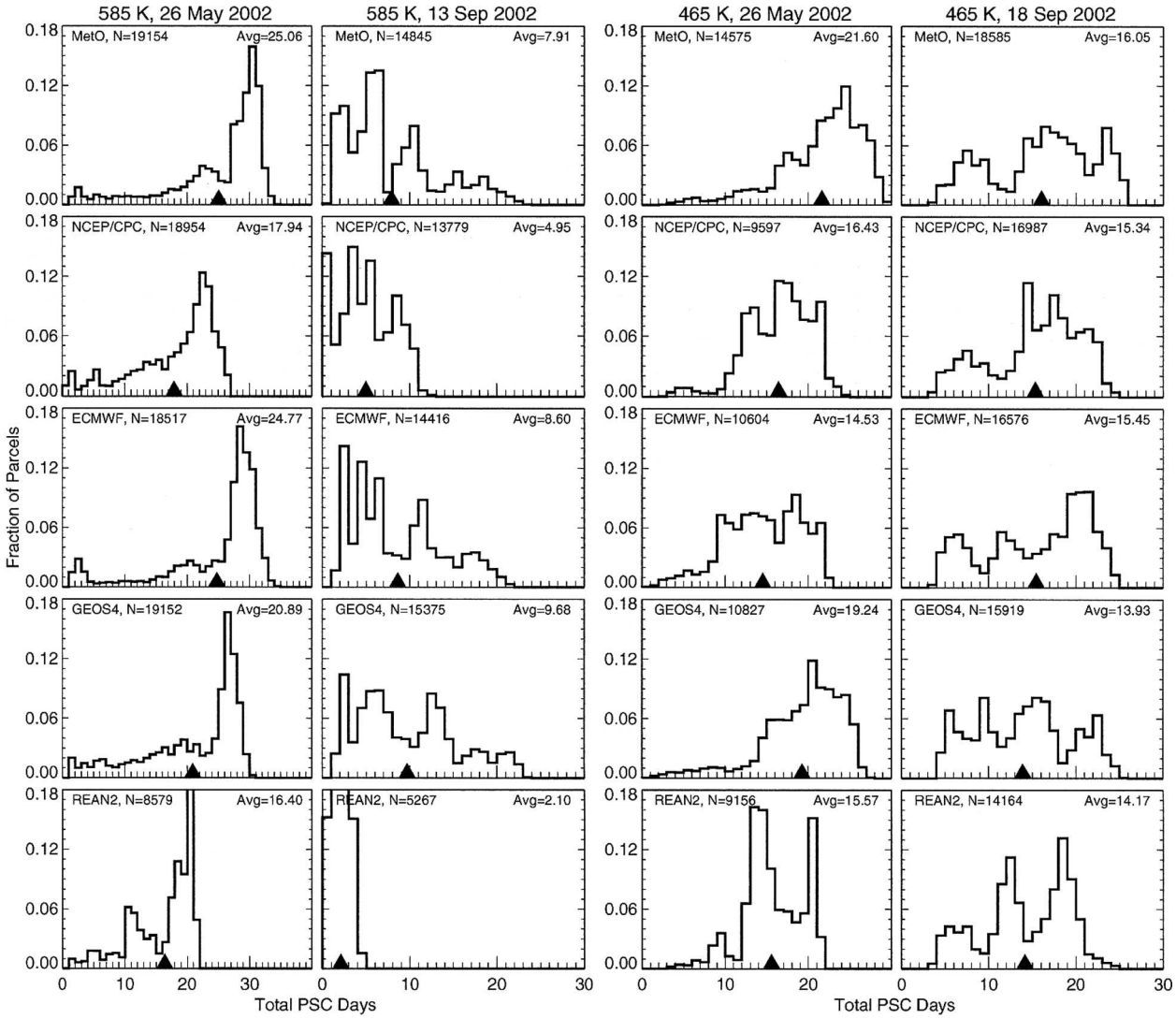

FIG. 12. Histograms of the total number of days spent at $T \leq T_{NAT}$ for trajectory runs initialized in the cold region at (left two columns) 585 and (right two columns) 465 K on (left) 26 May 2002 and (right) 13 and 18 Sep 2002. Arrows indicate average number of days; number of parcels used and average number of days are given in the labels. Note x axis for 26 May/585 K extends to 40 days, whereas others extend to 30 days.

spheric chemistry, quasi-isentropic transport and mixing, and large-scale dynamical evolution for four operational products (MetO, ECMWF, NCEP/CPC, and GEOS-4) as well as the ERA-40 and REAN/REAN-2 reanalyses to assess to what degree the conclusions of scientific studies may be affected by the choice of meteorological analysis.

While the comparisons overall provide a consistent picture of the large-scale dynamics of the SH 2002 winter between the analyses, indicating high confidence in many observational studies based on them, we have noted differences in several diagnostics that have the potential to significantly affect the outcome of studies using some of the analyses:

- REAN/REAN-2 lower-stratospheric temperatures are biased high and frequently indicate less pronounced extrema. The latter shortcoming is also seen in the NCEP/CPC data. ERA-40 Antarctic temperatures show persistent, unrealistic vertically oscillatory structure in the SH 2002 winter (Simmons et al. 2005) and additional degradation in August 2002.
- REAN/REAN-2 show weaker winds and EP flux divergence magnitudes in the top few levels at which they are available (between about 30 and 10 hPa).
- Substantial differences are seen in vortex strength, structure, and evolution in the upper stratosphere, with the NCEP/CPC objective analyses giving a cruder representation of these features, and the

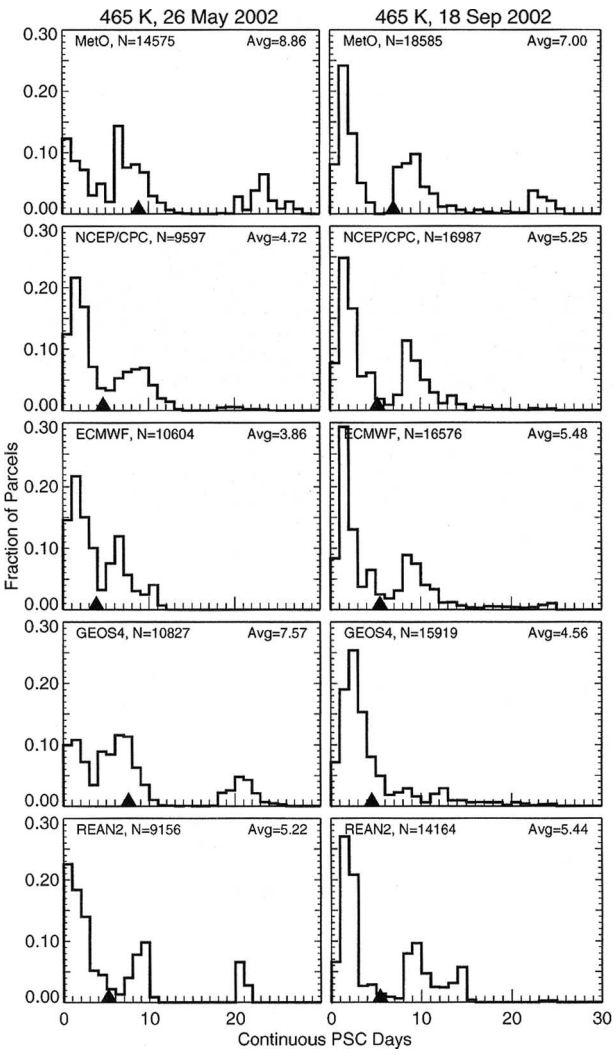

FIG. 13. Histograms of the number of days surrounding the initialization time continuously at $T \leq T_{NAT}$ for trajectory runs initialized in the cold region at 465 K on (left) 26 May 2002 and (right) 18 Sep 2002. Arrows indicate average number of days; number of parcels used and average number of days are given in the labels.

higher-resolution ECMWF and GEOS-4 analyses showing better representation of small structure, even when these analyses are used at reduced resolution.

- The polar vortex transport barrier is similar in all of the analyses, but there is little consensus on the amount, patterns, and timing of mixing in midlatitudes, or on the extent of mixing into the polar regions during the major warming. REAN-2 in particular shows less mixing in the lower stratosphere than the other analyses.
- ECMWF and GEOS-4 analyses (the higher-resolution assimilation systems considered here) represent filamentation and lamination in high-resolution transport calculations better than the other analyses.
- Temperature history calculations relevant to polar process modeling show the REAN/REAN-2 analyses to be an outlier, predicting significantly shorter PSC lifetimes and less potential for chlorine activation than the other analyses.

The comparisons presented here highlight limitations that make some of the datasets inappropriate for certain studies: The REAN/REAN-2 analyses were primarily designed for studying the troposphere (Kalnay et al. 1996); they have badly biased temperatures in the lower stratosphere and do not adequately represent dynamical events above ~50 hPa. The ERA-40 reanalyses also have unrealistic temperature structure in the polar lower stratosphere, and thus are inappropriate for detailed polar processing studies. The NCEP/CPC objective analyses have been very valuable in the past, facilitating groundbreaking studies of middle-atmosphere dynamics. However, compared to the assimilated datasets now available, they suffer from the assumptions that must be made in deriving dynamical fields.

The studies in which the effects of choosing one of these analyses are most critical, and most likely to influence the outcome, are detailed chemistry and transport modeling studies (including polar processing), as well as more detailed studies of synoptic evolution and finescale structure in dynamical fields (especially in the upper stratosphere). Some research efforts are already assessing these effects for the 2002 SH winter by driving models with more than one of these analyses (e.g., Feng et al. 2005; Manney et al. 2005). In the areas where there is the least consensus among the analyses—detailed 3D synoptic evolution, transport, mixing, and development of finescale structure—we currently have little data available to help to determine which results are most accurate. However, we are now seeing a dramatic increase in global, relatively high resolution, long-lived trace-gas observations and temperature data extending through the mesosphere from instruments on Environmental Satellite (ENVISAT) and Earth Observing System (EOS) Aura. These new observations will enhance our ability to quantitatively assess the accuracy of global meteorological datasets and that of the transport and model calculations that rely on them.

Acknowledgments. Thanks to the British Atmospheric Data Centre for providing MetO data and the GSFC ACD Science Data System (Eric Nash and Paul Newman) for providing NCEP/CPC data; NCEP reanalysis and reanalysis-2 data were provided by the NOAA–CIRES Climate Diagnostics Center, Boulder, Colorado, from their Web site at http://www.cdc.noaa.gov/. Data from the South Pole Ozonesonde Program are from http://www.cmdl.noaa.gov/ozwv/ozsondes/spo/ozppp2002.html. SAGE III data were obtained from the NASA Langley Research Center Atmospheric Sciences Data Center. We thank the JPL MLS team for technical assistance, data management, and computer

support; Paul Newman for original routines used to calculate PV; Kathrin Schöllhammer and Markus Kunze for obtaining and processing ECMWF ω data; Wesley Ebisuzaki for information on REAN/REAN-2 data; Sara Amina Sena for graphics, analysis, and data management assistance; Crystal Montoya for bibliography database maintenance; and three reviewers for their helpful comments. This work describes activities undertaken as part of the Stratospheric Processes and their Role in Climate (SPARC) Data Assimilation Working Group. Work at JPL/CalTech was done under contract with the National Aeronautics and Space Administration.

REFERENCES

Allen, D. R., and N. Nakamura, 2001: A seasonal climatology of effective diffusivity in the stratosphere. *J. Geophys. Res.,* **106,** 7917–7935.

——, and ——, 2003: Tracer equivalent latitude: A diagnostic tool for isentropic transport studies. *J. Atmos. Sci.,* **60,** 287–304.

——, R. M. Bevilacqua, G. E. Nedoluha, C. E. Randall, and G. L. Manney, 2003: Unusual stratospheric transport and mixing during the 2002 Antarctic winter. *Geophys. Res. Lett.,* **30,** 1599, doi:10.1029/2003GL017117.

Douglass, A. R., M. R. Schoeberl, R. B. Rood, and S. Pawson, 2003: Evaluation of transport in the lower tropical stratosphere in a global chemistry and transport model. *J. Geophys. Res.,* **108,** 4259, doi:10.1029/2002JD002696.

Dunkerton, T. J., and D. P. Delisi, 1986: Evolution of potential vorticity in the winter stratosphere of January-February 1979. *J. Geophys. Res.,* **91,** 1199–1208.

Fairlie, T. D. A., M. Fisher, and A. O'Neill, 1990: The development of narrow baroclinic zones and other small-scale structure in the stratosphere during simulated major warmings. *Quart. J. Roy. Meteor. Soc.,* **116,** 287–315.

——, R. B. Pierce, W. L. Grose, G. Lingenfelser, M. Loewenstein, and J. R. Podolske, 1997: Lagrangian forecasting during ASHOE/MAESA: Analysis of predictive skill for analyzed and reverse-domain-filled potential vorticity. *J. Geophys. Res.,* **102,** 13 169–13 182.

Feng, W., and Coauthors, 2005: Three-dimensional model study of the Antarctic ozone hole in 2002 and comparison with 2000. *J. Atmos. Sci.,* **62,** 822–837.

Finger, F. G., M. E. Gelman, J. D. Wild, M. L. Chanin, A. Hauchecorne, and A. J. Miller, 1993: Evaluation of NMC upper-stratospheric temperature analyses using rocketsonde and lidar data. *Bull. Amer. Meteor. Soc.,* **74,** 789–799.

Gelman, M. E., A. J. Miller, R. M. Nagatani, and C. S. Long, 1994: Use of UARS data in the NOAA stratospheric monitoring program. *Adv. Space Res.,* **14** (9), 21–31.

Gray, L. J., S. Sparrow, M. Juckes, A. O'Neill, and D. G. Andrews, 2003: Flow regimes in the winter stratosphere of the Northern Hemisphere. *Quart. J. Roy. Meteor. Soc.,* **129,** 925–945.

Grooß, J.-U., P. Konopka, and R. Müller, 2005: Ozone chemistry during the 2002 Antarctic vortex split. *J. Atmos. Sci.,* **62,** 860–870.

Hanson, D., and K. Mauersberger, 1988: Laboratory studies of the nitric acid trihydrate: Implications for the south polar stratosphere. *Geophys. Res. Lett.,* **15,** 855–858.

Harnik, N., R. K. Scott, and J. Perlwitz, 2005: Wave reflection and focusing prior to the major stratospheric warming of September 2002. *J. Atmos. Sci.,* **62,** 640–650.

Haynes, P., and E. Shuckburgh, 2000a: Effective diffusivity as a diagnostic of atmospheric transport. 1. Stratosphere. *J. Geophys. Res.,* **105,** 22 777–22 794.

——, and ——, 2000b: Effective diffusivity as a diagnostic of atmospheric transport. 2. Troposphere and lower stratosphere. *J. Geophys. Res.,* **105,** 22 795–22 810.

Kalnay, E., and Coauthors, 1996: The NCAR/NCEP 40-Year Reanalysis Project. *Bull. Amer. Meteor. Soc.,* **77,** 437–471.

Kanamitsu, M., W. Ebisuzaki, J. Woollen, S.-K. Yang, J. J. Hnilo, M. Fiorino, and G. L. Potter, 2002: NCEP–DOE AMIP-II reanalysis (R-2). *Bull. Amer. Meteor. Soc.,* **83,** 1631–1643.

Kistler, R., and Coauthors, 2001: The NCEP–NCAR 50-year reanalysis: Monthly means CD-ROM and documentation. *Bull. Amer. Meteor. Soc.,* **82,** 247–267.

Konopka, P., J.-U. Grooß, K. W. Hoppel, H.-M. Steinhorst, and R. Müller, 2005: Mixing and chemical ozone loss during and after the Antarctic polar vortex major warming in September 2002. *J. Atmos. Sci.,* **62,** 848–859.

Krüger, K., B. Naujokat, and K. Labitzke, 2005: The unusual midwinter warming in the Southern Hemisphere stratosphere 2002: A comparison to Northern Hemisphere phenomena. *J. Atmos. Sci.,* **62,** 603–613.

Lin, S.-J., 2004: A "vertically Lagrangian" finite-volume dynamical core for global models. *Mon. Wea. Rev.,* **132,** 2293–2307.

Lorenc, A. C., and Coauthors, 2000: The Met. Office global three-dimensional variational data assimilation scheme. *Quart. J. Roy. Meteor. Soc.,* **126,** 2991–3012.

Manney, G. L., J. D. Farrara, and C. R. Mechoso, 1994a: Simulations of the February 1979 stratospheric sudden warming: Model comparisons and three-dimensional evolution. *Mon. Wea. Rev.,* **122,** 1115–1140.

——, R. W. Zurek, A. O'Neill, and R. Swinbank, 1994b: On the motion of air through the stratospheric polar vortex. *J. Atmos. Sci.,* **51,** 2973–2994.

——, R. Swinbank, S. T. Massie, M. E. Gelman, A. J. Miller, R. Nagatani, A. O'Neill, and R. W. Zurek, 1996: Comparison of U.K. Meteorological Office and U.S. National Meteorological Center stratospheric analyses during northern and southern winter. *J. Geophys. Res.,* **101,** 10 311–10 334.

——, J. C. Bird, D. P. Donovan, T. J. Duck, J. A. Whiteway, S. R. Pal, and A. I. Carswell, 1998: Modeling ozone laminae in ground-based Arctic wintertime observations using trajectory calculations and satellite data. *J. Geophys. Res.,* **103,** 5797–5814.

——, H. A. Michelsen, F. W. Irion, M. R. Gunson, G. C. Toon, and A. E. Roche, 2000: Lamination and polar vortex development in fall from ATMOS long-lived trace gases observed during November 1994. *J. Geophys. Res.,* **105,** 29 023–29 038.

——, J. L. Sabutis, S. Pawson, M. L. Santee, B. Naujokat, R. Swinbank, M. E. Gelman, and W. Ebisuzaki, 2003: Lower stratospheric temperature differences between meteorological analyses in two cold Arctic winters and their impact on polar processing studies. *J. Geophys. Res.,* **108,** 8328, doi:10.1029/2001JD001149.

——, and Coauthors, 2005: Simulations of dynamics and transport during the September 2002 Antarctic major warming. *J. Atmos. Sci.,* **62,** 690–707.

Marchand, M., S. Bekki, A. Pazmino, F. Lefèvre, S. Godin-Beekmann, and A. Hauchecorne, 2005: Model simulations of the impact of the 2002 Antarctic ozone hole on midlatitudes. *J. Atmos. Sci.,* **62,** 871–884.

Newman, P. A. and E. R. Nash, 2005: The unusual Southern Hemisphere stratosphere winter of 2002. *J. Atmos. Sci.,* **62,** 614–628.

——, L. R. Lait, M. R. Schoeberl, R. M. Nagatani, and A. J. Krueger, 1989: Meteorological atlas of the Northern Hemisphere lower stratosphere for January and February 1989 during the Airborne Arctic Stratospheric Expedition. NASA Tech. Rep. 4145, 131 pp.

Pawson, S., K. Krüger, R. Swinbank, M. Bailey, and A. O'Neill, 1999: Intercomparison of two stratospheric analyses: Temperatures relevant to polar stratospheric cloud formation. *J. Geophys. Res.,* **104,** 2041–2050.

Randall, C. E., G. L. Manney, D. R. Allen, R. M. Bevilacqua, C. Trepte, W. A. Lahoz, and A. O'Neill, 2005: Reconstruction and simulation of stratospheric ozone distributions during the 2002 austral winter. *J. Atmos. Sci.,* **62,** 748–764.

Randel, W. J., 1987: The evaluation of winds from geopotential height data in the stratosphere. *J. Atmos. Sci.,* **44,** 3097–3120.

——, and Coauthors, 2004: The SPARC intercomparison of middle atmosphere climatologies. *J. Climate,* **17,** 986–1003.

Rogers, H. L., W. A. Norton, A. Lambert, and R. G. Grainger, 1999: Isentropic, diabatic, and sedimentary transport of Mount Pinatubo aerosol. *J. Geophys. Res.,* **104,** 4051–4063.

Roscoe, H. K., J. D. Shanklin, and S. R. Colwell, 2005: Has the Antarctic vortex split before 2002? *J. Atmos. Sci.,* **62,** 581–588.

Sabutis, J. L., 1997: The short-term transport of zonal mean ozone using a residual mean circulation calculated from observations. *J. Atmos. Sci.,* **54,** 1094–1106.

Scaife, A. A., R. Swinbank, D. R. Jackson, N. Butchart, H. Thornton, M. Keil, and L. Henderson, 2005: Stratospheric vacillations and the major warming over Antarctica in 2002. *J. Atmos. Sci.,* **62,** 629–639.

Schoeberl, M. R., A. R. Douglass, Z. Zhu, and S. Pawson, 2003: A comparison of the lower stratospheric age spectra derived from a general circulation model and two data assimilation systems. *J. Geophys. Res.,* **108,** 4113, doi:10.1029/2002JD002652.

Siegmund, P., H. Eskes, and P. van Velthoven, 2005: Antarctic ozone transport and depletion in austral spring 2002. *J. Atmos. Sci.,* **62,** 838–847.

Simmons, A. J., M. Hortal, G. Kelly, A. McNally, A. Untch, and S. Uppala, 2005: ECMWF analyses and forecasts of stratospheric winter polar vortex breakup: September 2002 in the Southern Hemisphere and related events. *J. Atmos. Sci.,* **62,** 668–689.

Sinnhuber, B.-M., M. Weber, A. Amankwah, and J. P. Burrows, 2003: Total ozone during the unusual Antarctic winter of 2002. *Geophys. Res. Lett.,* **30,** 1580, doi:10.1029/2002GL016798.

Swinbank, R., N. B. Ingleby, P. M. Boorman, and R. J. Renshaw, 2002: A 3D variational data assimilation system for the stratosphere and troposphere. Tech. Rep. 71, Met Office Numerical Weather Prediction Forecasting Research Scientific Paper, 33 pp.

Tan, W. W., M. A. Geller, S. Pawson, and A. da Silva, 2004: A case study of excessive subtropical transport in the stratosphere of a data assimilation system. *J. Geophys. Res.,* **109,** D11102, doi:10.1029/2003JD004057.